Strength and structural phase transitions of gadolinium at high pressure from radial X-ray diffraction

Lun Xiong, Jing Liu, Ligang Bai, Xiaodong Li, Chuanlong Lin, and Jung-Fu Lin

---

Strength and structural phase transitions of gadolinium at high pressure from radial X-ray diffraction

Lun Xiong,[1,a)] Jing Liu,[1] Ligang Bai,[1] Xiaodong Li,[1] Chuanlong Lin,[1] and Jung-Fu Lin[2]

[1]*Beijing Synchrotron Radiation Facility, Institute of High Energy Physics, Chinese Academy of Sciences, Beijing 100049, People's Republic of China*
[2]*Department of Geological Sciences, Jackson School of Geosciences, The University of Texas at Austin, Texas 78712, USA*

Lattice strength and structural phase transitions of gadolinium (Gd) were determined under nonhydrostatic compression up to 55 GPa using an angle-dispersive radial x-ray diffraction technique in a diamond-anvil cell at room temperature. Three new phases of fcc structure, dfcc structure, and new monoclinic structure were observed at 25 GPa, 34 GPa, and 53 GPa, respectively. The radial x-ray diffraction data yield a bulk modulus $K_0 = 36(1)$ GPa with its pressure derivate $K_0' = 3.8(1)$ at the azimuthal angle between the diamond cell loading axis and the diffraction plane normal and diffraction plane $\psi = 54.7°$. With K_0' fixed at 4, the derived K_0 is 34(1) GPa. In addition, analysis of diffraction data with lattice strain theory indicates that the ratio of differential stress to shear modulus (t/G) ranges from 0.011 to 0.014 at pressures of 12–55 GPa. Together with estimated high-pressure shear moduli, our results show that Gd can support a maximum differential stress of 0.41 GPa, while it starts to yield to plastic deformation at 16 GPa under uniaxial compression. The yield strength of Gd remains approximately a constant with increasing pressure, and reaches 0.46 GPa at 55 GPa. © *2014 AIP Publishing LLC*. [http://dx.doi.org/10.1063/1.4904747]

I. INTRODUCTION

At ambient conditions, the 4f shell of the regular trivalent rare earth elements from Pr to Lu (excluding Ce, Eu, and Yb) is gradually filled with increasing atomic number. The 4f electrons are in a highly localized state and do not participate in bonding.[1] The behavior of the 4f rare earth elements has been studied under compression for decades. The regular trivalent rare earth metals from La to Lu except Eu and Yb have been shown to follow a crystal structure sequence with increasing pressure: hcp → Sm-type → dhcp → fcc,[2] due to the d-electron character of the conduction band (s → d transition). At the completion of this sequence, the lanthanides undergo a phase transition from the fcc structure to a distorted fcc (dfcc) phase.[2–4]

Further compression experiments on several 4f rare earth elements (Ce,[5] Pr,[6,7] Gd,[8,9] and Dy[10]) have resulted in transitions from the dfcc structure to lower symmetry phases. These transitions are accompanied by a large volume collapse, related to 4f-electron delocalization induced by pressure.[11] However, there is a controversy about the structure of the low symmetry phases in Gd. Additionally, there is no direct experimental measurement on its strength. Previous studies have shown that the hardness of materials can be reflected in strength as it represents the contributions of both plastic and elastic deformation.[12]

The main goal of this work is to study the strength and structure of Gd at high pressures. We have performed *in situ* synchrotron angle dispersive radial x-ray diffraction

measurements in a two-fold panoramic diamond-anvil cell (DAC) under uniaxial compression up to 55 GPa. Together with the lattice strain theory,[13,14] we have obtained the strength and compression curve of Gd under nonhydrostatic compression.

II. EXPERIMENT

A commercially available Gd sample (purity of 99.9%) was purchased from Aladdin Chemistry Co. Ltd. For the radial x-ray diffraction (RXD) measurements, a two-fold panoramic DAC with a pair of beveled diamond anvils (300 μm culet) was used to exert uniaxial compression. A beryllium (Be) gasket was pre-indented to ∼40-μm thickness and drilled a hole of 50-μm-diameter in the center of the pre-indented area as the sample chamber. Special attention was paid to ensure that the sample hole was well centered with respect to the diamond anvil cell. A piece of Gd film with a diameter of ∼50 μm was loaded into the gasket hole and gold (Au) disk with a diameter of ∼20 μm was placed on the top within 5μm of the sample center, serving as a pressure standard[15] as well as the positioning reference for x-ray diffraction.[16] No pressure-transmitting medium was used. By design, the DAC was tilted by an angle of 28° to minimize the contribution of Be diffraction to the sample patterns (Fig. 1).[17] Angle dispersive RXD experiments were performed at the 4W2 beam line of Beijing Synchrotron Radiation Facility (BSRF), Chinese Academy of Sciences. A Si(111) monochromator was used to tune the synchrotron source to a wavelength of 0.6199 Å, and the incident monochromatic x-ray beam was focused by a pair of Kirkpatrick-Baez mirrors to an approximately 36 (vertical) $\times$ 15 (horizontal) μm^2

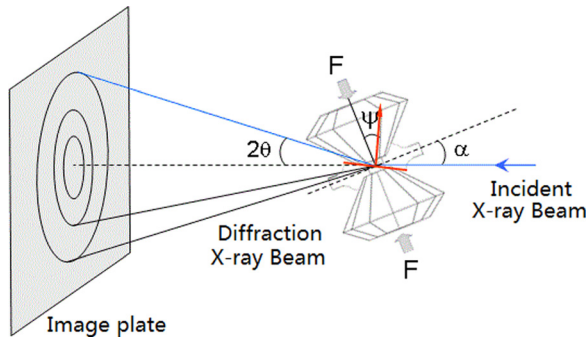a)Author to whom correspondence should be addressed. Electronic mail: xionglun@ihep.ac.cn

FIG. 1. Schematic experimental setup for angle-dispersive radial x-ray diffraction coupled with a DAC. The DAC was tilted by an angle of $\alpha = 28°$.

full width at half maximum (FWHM) spot and directed through the Be gasket and the sample. Two-dimensional diffraction patterns were collected by a Mar345 image plate detector and analyzed with the program Fit2D.[18] The sample-to-detector distance and orientation of the detector were calibrated by a CeO_2 standard. At each pressure, the RXD pattern was collected after sufficient time (about 30 min) of stress relaxation, and the data collecting time were 20–25 min for a single spectrum.

III. THEORY

The radial x-ray diffraction data were analyzed using the lattice strain theory developed by Singh and co-workers.[13,14] According to the lattice strain theory, the measured d-spacing $d_m(hkl)$ is a function of the azimuthal angle ψ between the DAC loading axis and the diffraction plane normal (hkl), and can be calculated as

$$d_m(hkl) = d_p(hkl)[1 + (1 - 3\cos^2\psi)Q(hkl)], \quad (1)$$

where $d_m(hkl)$ is the measured d-spacing, $d_p(hkl)$ is the d-spacing under equivalent hydrostatic pressure, and $Q(hkl)$ is the orientation dependent lattice strain.

Under isostress conditions (the Reuss limit), the differential stress, t, can be expressed as

$$t = 6G\langle Q(hkl)\rangle, \quad (2)$$

where $\langle Q(hkl)\rangle$ represents the Q value averaged over all observed reflections, and G is the aggregate shear modulus of the polycrystalline sample. The pressure dependence of G can be obtained from extrapolation of ultrasonic or theoretically calculated single-crystal elastic constants. If the differential stress t has reached the limit of yield strength at high pressures when materials start to deform plastically, $6\langle Q(hkl)\rangle = t/G$ will reflect the ratio of yield strength to shear modulus. In addition, this ratio can be a good qualitative indicator of hardness as it reflects the contributions of both plastic and elastic deformation.[12]

Equation (1) indicates that the $d_m(hkl)$ versus $(1 - 3\cos^2\psi)$ plot is a straight line for given $d_p(hkl)Q(hkl)$, and its slope, $d_p(hkl)Q(hkl)$, is directly related to $t/G = 6\langle Q(hkl)\rangle$. $d_p(hkl)$ is normally at $\psi = 54.7°$. With additional, independent constraints on the high-pressure shear modulus, the differential stress or yield strength at high pressure can be determined.

For the conventional RXD experiments, the incident x-ray beam is perpendicular to the compression axis and passes through a Be gasket and the Be gasket contributes intense diffraction lines to the sample patterns. Thus, we tilt the DAC to an angle of α between the compression axis and the incident x-ray to minimize the Be contribution to the sample patterns ($\alpha = 28°$). In this geometry, ψ in Eq. (1) can be rewritten as[19]

$$\cos\psi_{hkl} = \sin\alpha\cos\delta\cos\theta_{hkl} + \cos\alpha\sin\theta_{hkl}, \quad (3)$$

where θ is the diffraction angle and δ is the azimuthal angle on the plane of the detector.

IV. RESULTS AND DISCUSSION

The RXD diffraction patterns are integrated over each azimuthal sector with a 5° interval using Fit2D.[18] The program Multifit 4.2 is used to perform macro decomposition of the 2D diffraction images into azimuthal slices within Fit2D,[18] yielding one-dimensional plots of x-ray intensity as a function of 2θ, as well as peak positions, intensities, and FWHM of the diffraction peaks. To determine the variation of the diffraction peak positions with δ, we integrated the diffraction patterns with segments of 5° in the azimuth angle, in the range of 180°–270°, and fitted peak positions. RXD spectra of Gd were collected up to an equivalent pressure of 55 GPa, where pressures were derived from the equation of state of Au[15] with the unit cell volume obtained from $d_p(111)$ of Au at $\psi = 54.7°$.

Fig. 2 shows the selected diffraction patterns of the sample taken at $\psi_{hkl} = 54.7°$ under different pressures. The dhcp-fcc transition was found at 25 GPa and fcc-dfcc transition at 34 GPa, in good agreement with previous energy dispersive x-ray diffraction (EDXRD) studies performed by Grosshans and Holzpafel,[3] and angle DXRD (ADXRD) studies performed by Errandonea et al.[9] Another phase transition
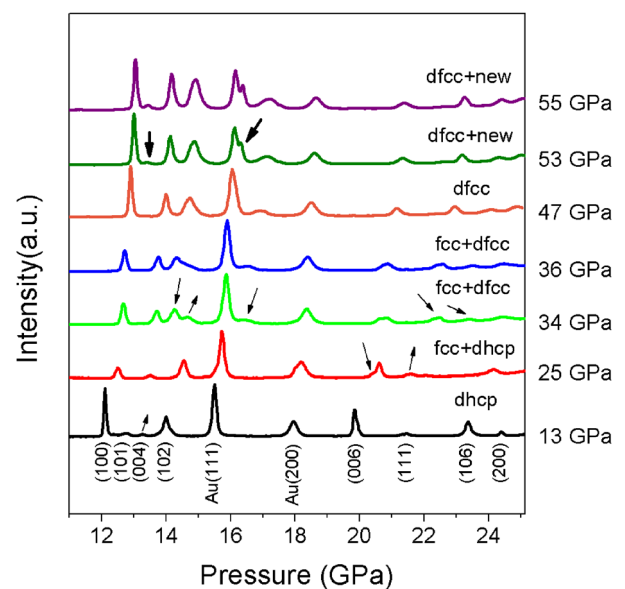

FIG. 2. Representative diffraction patterns of Gd under nonhydrostatic compression at $\psi = 54.7°$. The pressures are determined from Au(111) at $\psi = 54.7°$.

was observed at 53 GPa, smaller than the previous results: 58 GPa,[3] 59 GPa,[8] 60.5 GPa,[9] and 60 GPa.[20] As there was no pressure medium, the transition pressure was forced earlier near 10% than previously reports. The diffraction pattern remains nearly the same at 53 GPa except for the appearance of two new peaks (depicted by bold arrows) caused by the onset of the dfcc-new phase transition.

The distorted fcc phase structure obtained at 39 GPa is identified with the trigonal space group $R\bar{3}m$ with lattice parameters $a = 6.129(11)$ and $c = 15.191(12)$, consistent with the previous results.[9] The new phase of Gd was previously assigned to the monoclinic bcm structure ($I2/m$) proposed by Hua *et al.*[20] and monoclinic post-dfcc phase ($C2/m$) recommended by Errandonea *et al.*[9] Unfortunately, there are not sufficient diffraction peaks to solve the structure of new monoclinic phase appeared at 53 GPa.

The d-spacing as a function of $1 - 3\cos^2\psi$ for selected diffraction peaks of Gd at seven selected pressures are shown in Fig. 3. As expected from the theory,[13,14] the measured d-spacing for all diffraction peaks shows a linear relationship with $1 - 3\cos^2\psi$.

The d-spacings determined at $(1 - 3\cos^2\psi) = 0$ with $\psi = 54.7°$ were used for least-squares fitting to calculate the mean lattice parameters and the equivalent unit cell volumes. The normalized unit cell volume of compression curves for $\psi = 0°$, $\psi = 54.7°$, and $\psi = 90°$ are shown in Fig. 4. For comparison, the results obtained from previous works were also included.[3,9,21–24]

The unit cell volumes as a function of pressure were fitted using third-order Birch–Murnaghan equation of state (EoS) to obtain the ambient pressure bulk modulus K_0 and its pressure derivate K_0'.[25] The third-order Birch–Murnaghan EoS is expressed as follows:[26]

$$P = 1.5 K_0 \left[\left(\frac{V_0}{V}\right)^{\frac{7}{3}} - \left(\frac{V_0}{V}\right)^{\frac{5}{3}} \right] \left\{ 1 + \frac{3}{4}(K_0' - 4)\left[\left(\frac{V_0}{V}\right)^{\frac{2}{3}} - 1 \right] \right\},$$

(4)

FIG. 4. Pressure-volume relations of Gd derived from $\psi = 0°$, 54.7°, and 90°, respectively. Solid lines represent the Birch-Murnaghan equation fits to the data at each given ψ angle. Literature compressional data of Gd are also shown for comparison.

where K_0, K_0', and V_0 are the bulk modulus, its pressure derivate, and the unit-cell volume at ambient conditions, respectively. Through fitting the diffraction data at $\psi = 54.7°$ to 55 GPa by Eq. (4), we obtain the bulk module $K_0 = 36(1)$ GPa and its pressure derivative $K_0' = 3.8(1)$.

With K_0' fixed at 4, the least-squares fit yields an ambient bulk modulus $K_0 = 34(1)$ GPa. The bulk modulus obtained from fits of diffraction data at $\psi = 0°$ and 90° are 27(1) GPa and 43(2) GPa, respectively. Angles $\psi = 0°$ and 90° represent the diffracting plane normal parallel and perpendicular to the loading axis, with maximum and minimum stresses, respectively. The bulk moduli gradually increased from $\psi = 0°$ to $\psi = 90°$, showing the compressibility of the sample strongly depends on the stress environment.

A comparison between our research results and the previously reported data[3,9,22–24,27–32] on the bulk modulus (K_0) and its pressure derivative (K_0') is shown in Table I. It can be seen that the bulk modulus of Gd obtained here under uniaxial compression at $\psi = 54.7°$ is in highly consistent
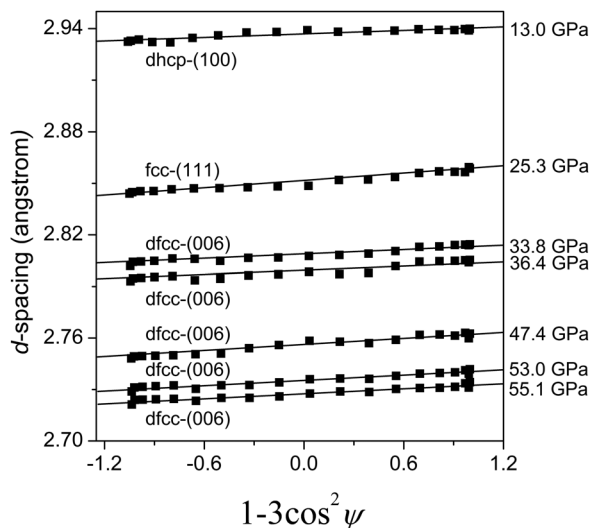

FIG. 3. Observed d-spacings versus $1 - 3\cos^2\psi$ at seven representative pressures. Solid lines represent least-squares linear fits to the data. The pressures are determined form Au(111) at $\psi = 54.7°$.
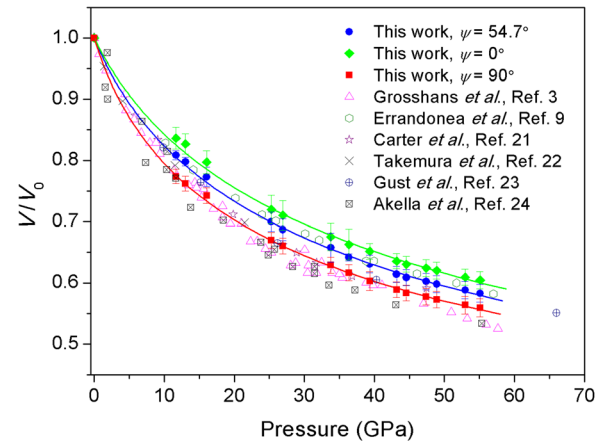
TABLE I. A summary of the bulk modulus (K_0) of Gd and its pressure derivative (K_0') obtained from various methods. RXD; XRD; and PTM: pressure-transmitting medium.

K_0 (GPa)	K_0'	P_{max} (GPa)	Method and PTM	Reference
34(1)	4(fixed)	55	RXD ($\psi = 54.7°$), null	This work
36(1)	3.8(1)		RXD ($\psi = 54.7°$), null	
27(1)	4.2(1)		RXD ($\psi = 0°$), null	
43(2)	3.7(2)		RXD ($\psi = 90°$), null	
35	2.9	40	XRD, nitrogen	Grosshans[3]
34(3)	4.2(2)	60.5	XRD, argon	Errandonea[9]
34	3.2	21	XRD, silicone oil	Takemura[22]
39		115	Shock wave, null	Gust[23]
23(2)	4.3(3)	106	XRD, silicone oil	Akella[24]
37	2.3	…	…	Grosshans[27]
36	6.0	…	…	Bridgman[28]
36	4.8	4.5	Shock wave, null	Vaidya[29]
39		…	…	Weik[30]
38		…	…	Spedding[31]
38	3.3	0.5	Ultrasonic wave, null	Fisher[32]

with the results obtained from experiments as well as theoretical calculation (34–39 GPa),[3,9,22,23,27–32] except for the value of 23 GPa obtained from Akella *et al.*[24] The differences may be due to different starting samples, and/or hydrostaticity. The pressure derivative obtained from the third-order Birch-Murnaghan EoS is close to 4 and the values of K_0 are highly consistent with independent studies.

According to Eq. (1), the orientation dependent lattice strain $Q(hkl)$ can be derived from the slope of the linear relationship between the observed d spacing and $1 - 3\cos^2\psi = 0$. The ratio of t/G was obtained from averaged value of $Q(hkl)$ over all observed reflections. Fig. 5 displays t/G as a function of pressure for Gd. For Gd, the ratio of t/G ranges from 0.011 to 0.014 at pressures of 12–55 GPa with an average value of 0.014. The ratio of t/G remains constant above ∼16 GPa, indicating that Gd undergoes plastic deformation and t/G reaches its limit of 0.014 at this pressure. This ratio might be a good qualitative indicator of hardness as it reflects the contributions of both plastic and elastic deformation. In addition, the ratio of t/G of Gd obtained at high pressures is close to the value of W obtained by He *et al.*[12]

With the high-pressure shear modulus known, the differential stress can be derived at each pressure step from $t = 6G\langle Q(hkl)\rangle$. The volume dependent shear modulus G of the polycrystalline aggregate is given by

$$G = G_0(1 + 2f)5/2[1 + (3K_0 G_0'/ - 5)f], \qquad (5)$$

where $f = [(V_0/V)^{2/3} - 1]$ and K_0 is the bulk modulus at ambient pressure. Using the single-crystal elastic modulus,[33] the G values of tungsten at high pressures were derived from Eq. (5) as a function of different V_0/V.

For comparison, the differential stresses versus pressure determined form x-ray diffraction in a radial geometry for several reported metals (Mo,[34] Re,[35] Au,[34,35] W,[12] and Nb[36]) are plotted in Fig. 6. It can be seen that, the differential stress, t, remains almost unchanged above ∼16 GPa, indicating that Gd begins to experience macro yield with plastic deformation and t reaches its limited value of 0.41 GPa of

FIG. 6. Differential stress as a function of pressure for Gd, W, Au, Re, Mo, and Nb.

yield strength at this pressure. And the yield strength of Gd reaches a value of 0.46 GPa at 55 GPa. Obviously, the high-pressure strength of Gd is comparable to Au[34,35] and Nb;[36] while, the differential stress sustained by Gd is much less than W,[12] Mo,[34] and Re.[35] Unfortunately, there is almost no clear correlation between the differential stress and phase transition as the strength of Gd remains almost constant above ∼16 GPa.

V. CONCLUSION

We have determined the strength and compression behaviors of Gd in a diamond anvil cell under nonhydrostatic compression up to 55 GPa at room temperature using radial x-ray diffraction technique together with the lattice strain theory. The compression curve obtained at $\psi = 54.7°$ yields a bulk modulus $K_0 = 36(1)$ GPa and its pressure derivative $K_0' = 3.8(1)$. The bulk modulus under $\psi = 54.7°$ is in good agreement with previous results obtained from experiments as well as theoretical calculation. The differential stress supported by Gd ranges from 1.1% of the shear modulus at 12 GPa to 1.4% at 55 GPa. Given the estimation of the shear modulus at high pressures, the supported differential stress ranges from 0.31 GPa at 12 GPa to 0.46 GPa at 55 GPa. The change of t with pressure indicates that Gd starts to yield with plastic deformation and reaches its limiting value of 0.41 GPa at a nonhydrostatic compression of ∼16 GPa. The differential stress supported by Gd at high pressures is comparable to those of Au and Nb.
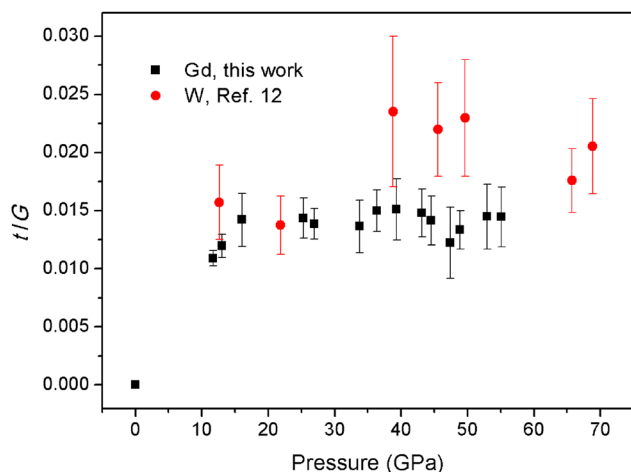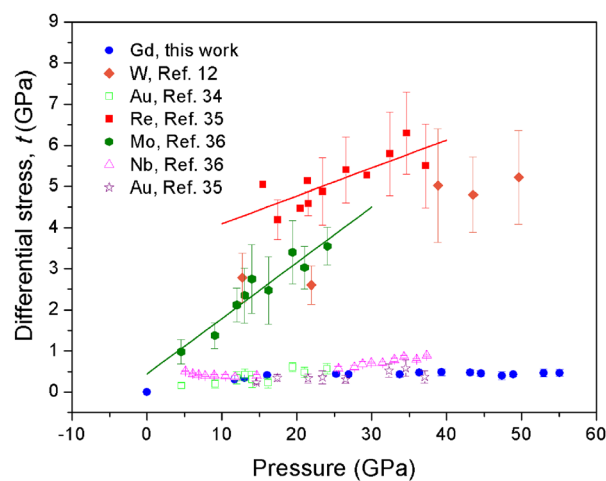
ACKNOWLEDGMENTS

FIG. 5. Ratio of the differential stress to the shear modulus (t/G) as a function of pressure for Gd and W. Pressures of Gd sample were determined from the Au pressure standard using (111) diffraction line at $\psi = 54.7°$ The errors are estimated from the scatter of $d(hkl)$ vs $1 - 3\cos^2\psi$.

[1]K. A. Gschneider and L. R. Eyring, *Handbook on the Physics and Chemistry of Rare Earths* (North-Holland, Amsterdam, 1993), Vol. 17.

[2]W. B. Holzapfel, J. Alloys Compd. **223**, 170 (1995).

[3]W. A. Grosshans and W. B. Holzapfel, Phys. Rev. B **45**, 5171 (1992).

[4]N. Hamaya, Y. Sakamoto, H. Fujihisa, Y. Fujii, K. Takemura, T. Kikegawa, and O. Shimomura, J. Phys.: Condens. Matter **5**, L369 (1993).

[5]K. A. Gschneider, Jr., R. O. Elliot, and R. R. McDonald, J. Phys. Chem. Solids **23**, 555 (1962).

[6]B. J. Baer, H. Cynn, V. Iota, C. S. Yoo, and G. Shen, Phys. Rev. B **67**, 134115 (2003).

[7]N. C. Cunningham, N. Velisavljevic, and Y. K. Vohra, Phys. Rev. B **71**, 012108 (2005).

[8]J. Akella, G. S. Smith, and A. P. Jephcoat, J. Phys. Chem. Solids **49**, 573 (1988).

[9]D. Errandonea, R. Boehler, B. Schwager, and M. Mezouar, Phys. Rev. B **75**, 014103 (2007).

[10]R. Patterson, C. K. Saw, and J. Akella, J. Appl. Phys. **95**, 5443 (2004).

[11]B. R. Maddox, A. Lazicki, C. S. Yoo, V. Iota, M. Chen, A. K. McMahan, M. Y. Hu, P. Chow, R. T. Scalettar, and W. E. Pickett, Phys. Rev. Lett. **96**, 215701 (2006).

[12]D. W. He and T. S. Duffy, Phys. Rev. B **73**, 134106 (2006).

[13]A. K. Singh, J. Appl. Phys. **73**, 4278 (1993).

[14]A. K. Singh and C. Balasingh, J. Appl. Phys. **75**, 4956 (1994).

[15]O. L. Anderson, D. G. Isaak, and S. Yamamoto, J. Appl. Phys. **65**, 1534 (1989).

[16]S. R. Shieh, T. S. Duffy, and B. S. Li, Phys. Rev. Lett. **89**, 255507 (2002).

[17]A. K. Singh, J. Phys. Chem. Solids **65**, 1589 (2004).

[18]A. P. Hammersley, S. O. Svensson, M. Hanfland, A. N. Fitch, and D. Häusermann, High Pressure Res. **14**, 235 (1996).

[19]S. Merkel, H. R. Wenk, J. F. Shu, G. Y. Shen, P. Gillet, H. K. Mao, and R. J. Hemley, J. Geophys. Res. **107**, 2271, doi:10.1029/2001JB000920 (2002).

[20]H. Hua, Y. K. Vohra, J. Akella, S. T. Weir, R. Ahuja, and B. Johansson, Rev. High Pressure Sci. Technol. **7**, 233 (1998).

[21]W. J. Carter, J. N. Fritz, S. P. Marsh, and R. G. McQueen, J. Phys. Chem. Solids **36**, 741 (1975).

[22]K. Takemura and K. Syassen, J. Phys. F **15**, 543 (1985).

[23]W. H. Gust and E. B. Royce, Phys. Rev. B **8**, 3595 (1973).

[24]J. Akella, G. S. Smith, and A. P. Jephcoat, J. Phys. Chem. Solids **49**, 573 (1988).

[25]R. Jeanloz and B. K. Godwal, J. Phys. Conf. Ser. **377**, 012032 (2012).

[26]F. Birch, J. Geophys. Res. **83**, 1257, doi:10.1029/JB083iB03p01257 (1978).

[27]W. A. Grosshans, Ph.D. thesis, University of Paderborn, 1987.

[28]P. W. Bridgman, *Collected Experimental Papers* (Harvard University Press, Cambridge, 1964).

[29]S. N. Vaidya and G. C. Kennedy, J. Phys. Chem. Solids **31**, 2329 (1972).

[30]H. Weik and K. Strnat, in *Landoldt Bornstein 6*, Auflage Band IV 2c (Springer–Verlag, Berlin, 1965), p. 626.

[31]F. H. Spedding, in *CRC Handbook of Chemistry and Physics*, 59th ed., edited by R. C. Weast and M. J. Astle (CRC Press, West Palm Beach, Florida, 1979), p. B261.

[32]E. S. Fisher, M. I. Manghnani, and R. Kikuta, J. Phys. Chem. Solids **34**, 687 (1973).

[33]S. Sindhu and C. S. Menon, Pramana-J. Phys. **47**, 435 (1996).

[34]T. S. Duffy, G. Y. Shen, J. F. Shu, H. K. Mao, R. J. Hemley, and A. K. Singh, J. Appl. Phys. **86**, 6729 (1999).

[35]T. S. Duffy, G. Y. Shen, D. L. Heinz, J. F. Shu, Y. Z. Ma, H. K. Mao, R. J. Hemley, and A. K. Singh, Phys. Rev. B **60**, 15063 (1999).

[36]A. K. Singh and H. P. Liermann, J. Appl. Phys. **109**, 113539 (2011).